

EPSC2017

LP1 abstracts

A Novel Method for Forming a Hyperspectral Image

C.E. Huntly (1), D. Langstaff (1), M. Gunn (1), R. Cross (1), L. Tyler (1), A.P. Gay (2), C. Cousins (3)

(1) Institute of Mathematics, Physics and Computer Science, Aberystwyth University.

(2) Institute of Biological, Environmental and Rural Sciences, Aberystwyth University

(3) Earth and Environmental Science, University of St Andrews

Introduction

Spectral imaging is the combination of the fields of spectroscopy and imaging; there are two non-distinct areas of spectral imaging classified by the number of spectral bands the imager is capable of taking. Multispectral imagers capture discrete areas of the spectrum, typically selected for specific science outputs. Hyperspectral imagers build up sufficient spectral bands to form a contiguous spectrum. The data is stored in a three dimensional image cube, where each pixel contains a complete spectrum. The dimensions in an image cube represent the traditional x and y dimensions in the two dimensional spatial frame, with the third dimension, λ , representing the spectral information.

There are multiple existing techniques that build up these image cubes, as shown in Figure 1. Those detailed here are:

- **Whiskbroom**

A single point is scanned across the x and y frames by moving either the sample or the detector. [Li et al., 2013]

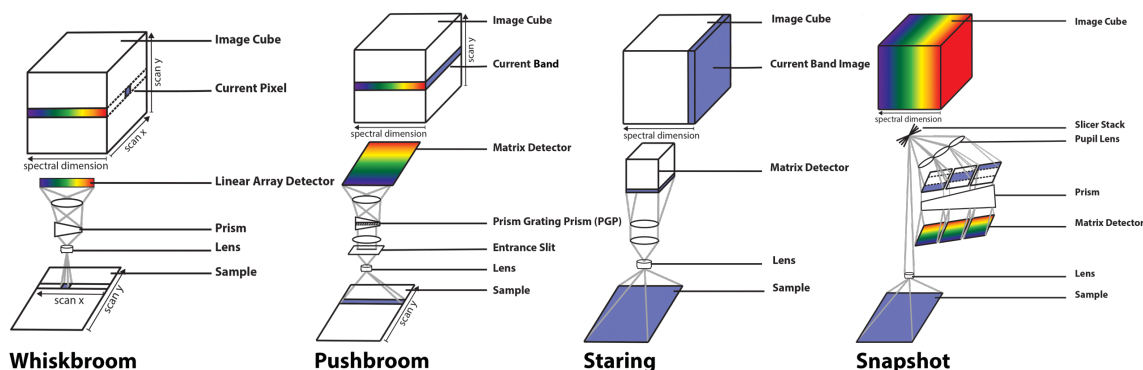


Figure 1: Existing Spectral Imaging Techniques. Adapted from [Li et al., 2013]

- **Pushbroom**

A line scan is gathered across one axis and spectral information is obtained by spectrally dispersing the image creating a 2D image with spatial information on one axis and spectral on the other. A series of scans is then taken to complete the image cube. [Aiazzi et al., 2006]

- **Staring**

A dispersion element such as a fixed bandpass filter or a linear variable filter (LVF) is used to capture a narrowband of the spectrum. A series of 2D images build up the image cube. [Gupta, 2011]

- **Snapshot**

Both spectral and spatial information is recorded in one exposure using a slicer stack and a series of lenses and detectors. [Li et al., 2013]

Multispectral and Hyperspectral Imagers are particularly useful for space applications; for example, in planetary exploration where spectroscopy studies can be more easily carried out by camera systems than by spectrometer

equipment primarily held in the body of a rover. The relatively small data sets are sent back to Earth and processed through existing imaging processing pipelines. Hyperspectral Imaging was however developed initially for remote sensing purposes; still it's primary use today [Goetz, 2009].

Instrumentation

The proposed new technique of hyperspectral imager being developed in Aberystwyth is a windowing-pushbroom camera system, SPEC-I. It is fitted with a LVF in an actuator making it possible to cover a wide range of wavelengths in a small imaging system.

The image can be built up in two ways, shown in Figure 2, the first is to fix the linear variable filter over a desired wavelength range and then either move the camera or the subject. The second method of gaining a hyperspectral image set is to scan the LVF across the optical path, keeping both the camera and the subject stationary. The image cube is built up over a series of 2D frames.

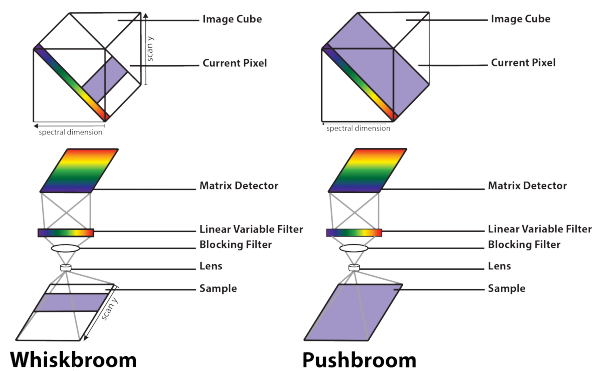


Figure 2: Aberystwyth Novel Hyperspectral Imager - SPEC-I

Application Area

SPEC-I is a hyperspectral imager that has been delivered as part of continued collaborative work with the UK Space Agency under Crest 2. It is a functioning field camera designed with agricultural purposes in mind. As such it has a spectral range that includes the Near Infrared, essential for plant diagnostics. NIR is essential because of the "red-edge" that can be used as a diagnostic

tool in plants, to the level where farmers can pin-point levels of nitrogen or water required at a plant specific level. [Boggs et al., 2003]

Preliminary Results

Back down to Earth SPEC-I has been initially tested in partnership with the Institute of Biological, Environmental & Rural Sciences. A plant that had both healthy and damaged material was imaged from 500 – 1100nm. The healthy spectrum shown in Figure 3 is indicative of a healthy "red edge". It is clear from the damaged spectrum that it does not adhere to the "red-edge" and has peaks that may be indicative of certain causes of damage.

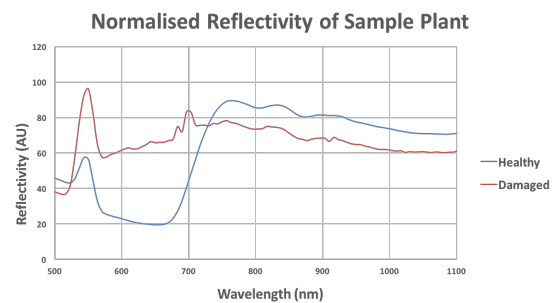


Figure 3: Initial Results from Plant Damage Investigation

Reference:

- [Li et al., 2013] Li, Q., He, X., Wang, Y., Liu, H., Xu, D., and Guo, F. (2013). Review of spectral imaging technology in biomedical engineering: achievements and challenges. *J Biomed Opt*, 18(10):100901.
- [Aiazzi et al., 2006] Aiazzi, B., et al.(2006). Noise modelling and estimation of hyperspectral data from airborne imaging spectrometers. *Annals of Geophysics*, 49(1):1-9.
- [Gupta, 2011] Gupta, N. (2011). Development of staring hyperspectral imagers. pages 1-8.
- [Goetz, 2009] Goetz, A. F. H. (2009). Three decades of hyperspectral remote sensing of the Earth: A personal view. *Remote Sensing of Environment*, 113(SUPPL. 1):S5-S16.
- [Boggs et al., 2003] Boggs, J. L., et al. (2003). Relationship between hyperspectral reflectance, soil nitrate-nitrogen, cotton leaf chlorophyll, and cotton yield: A step toward precision agriculture. *Journal of Sustainable Agriculture*, 22(3):5-16.

Challenges of Dawn FC data Photometry of Ceres

M. Hoffmann, A. Nathues, G. Thangjam, J. Ripken, T. Platz.
MPI for Solar System Research, Göttingen, Germany, (hoffmann@mps.mpg.de, +49 551 384 979 308).

Abstract

We discuss non-instrumental systematic deviations from global photometric properties in specific contexts. Besides resolution based influences the high dynamic range of reflectances, local constitutional properties of the surface and superposed semitransparent materials affect the scattering of light. Among others, the complicated case of crater Occator on Ceres requires most careful assessment of the true local photometric model, in contrast to an immediate application of a global model. Problems, methods and limitations of analysis are addressed.

1. Introduction

Proper interpretation of surface details based on images of the Dawn Framing Camera (FC) depends on a reliable photometric model that is used to correct reflectance values. FC images show Ceres resolved on a very wide range of resolutions from 9 to 27000 pixels per diameter which had to be modeled successively to derive Hapke parameters. Also ground-based unresolved photometric data [1] has been included in the determination of a global photometric model. Comparison of photometrically corrected data of specific locations revealed differences, if they were obtained from orbits characterized by different resolution. Also large differences in reflectance led to discrepancies, as well as locations with unusual geologic properties. Thus, the need for local individual correction became obvious.

2. Model approaches for Ceres' crater Occator

Using a global model for photometric correction, contrasts of reflectances reach a factor of 15 [2]. The associated geologic features indicate the presence of

quite diverse topographic and macroscopic roughness on different scales. As shown by [3] and [4], there is a variable surplus of scattered light to that of an undisturbed surface, which has been attributed to an optically thin haze. Because of this variability and the constraints from orbital geometry of the spacecraft, the improvement of photometric modeling can only be derived from the target data themselves, not from independent data. As long as the deviations from the model are small compared with the signal, iterative and heuristic approaches can be applied. These are: Investigate relative ratios of reflectances at selected locations inside and outside target, analyse contrasts, and separate phase effects from projection effects and optical depths. A consequence of the enhanced number of influencing variables is the failure of common photometric planetary surface models. Therefore additional appropriate parameters have to be included. Assuming specific layer sizes and distributions of, e.g., optical depths or grain sizes can help to describe a local context consistently. We are going to show examples of these complications and respective improvements of local photometric correction.

References

- [1] Reddy, V., et al., *Icarus* 260, 332-345, 2015.
- [2] Nathues, A., et al., *Planet. Space Sci.* 134, 122-127, 2016.
- [3] Nathues, A., et al., *Nature* 528, 237-240, 2015.
- [4] Thangjam, G. S., et al., *Astrophys. J.* 833, L25, 2017.

Earth-based detection of levitated lunar dust

M. Hoffmann (1)
(1) Weidenbach, Germany (hoffmann@mps.mpg.de)

Abstract

Lunar horizon glow analogue to Surveyor images has been detected from ground at high phase angles.

1. Introduction

The existence of electrostatically levitated dust on the Moon and other atmosphere-less bodies of the solar system has been frequently discussed (e.g. [1], [2]). Observations from the surface of the Moon and in orbit near the supersolar point support this concept [3], but Earth-based evidence seems to be missing yet. From the distance of the Earth, the moon-based localized glow near horizon may become global, since the phase angle is almost the same at its horizon. A reliable data base showing this phenomenon might help to understand transport processes of small-grained material and their dependence on regolith properties and solar irradiation. A theoretical model of the distribution of levitated dust on global scales has been published by [4]. It expands earlier results by [5]. Additional studies have been published by [1], [6], and [2]. Near new moon crescents are characterized by contrast to the twilight, and influenced by extinction and scintillation from the terrestrial atmosphere. Lunar topography and surface roughness causes shrinking of the sunlit arc when the phase angle increases [7], but a levitated layer of dust may enhance it.

2. Observations and results

In order to test the reality of a visual impression of an “iridescent” border of the Earth-lit disk of the moon by unaided eye, observable near new moon, videos were recorded using several ordinary commercial cameras at several geometrically favourable opportunities between 2006 and 2016 at different locations. Optimum observing conditions involve minimized atmospheric scattering, and an optimized

combination of (positive) lunar and (negative) solar angular altitude relative to an obstacle-free horizon. The observations presented here were obtained between 0 and 500 m height above sea level in Germany and Turkey. Positive detections were made for lunar phase angles between 160° and 170° . The lower limit is set by the disappearance of the phenomenon due to missing illumination of scattering particles and the upper limit by loss of contrast due to terrestrial atmospheric light. Scintillation is a minor problem, since it statistically lowers or even increases the contrast. For support, images from popular magazines and internet-based images were successfully compared, but their dynamic range is frequently not useful.

Besides the limitations imposed by the twilight and terrestrial atmosphere, also the illumination conditions at the Moon restrict the interval of possible observations. Near new moon the lunar limb which is averted from the Sun is still close to being illuminated by the Sun. Thus any dust floating above this part of the surface is reached by sunlight at low elevations. But the corresponding elevation limit (Sun at or above the local lunar horizon) changes more and more rapidly, as the phase angle decreases. A limit of observability is reached for a phase angle of 160° , when this elevation is about 28 km above the surface. At this elevation the density of the expected dust becomes very low, and only small particles are expected. Simultaneously, the optical path length across a dust layer of a density sufficient for an Earth-based detection also decreases. Furthermore, forward scattering of small particles becomes less effective. All this contributes to a rapid vanishing of conditions useful for observation at lunar equatorial latitudes. Near the lunar poles, the elevation of illuminated dust above the surface does not change much. Here an extension of the cusps of the crescent remains visible for phase angles somewhat below 160° . In total, there is an optimum interval of phase angles for Earth-based detections. Experience has shown that this interval ranges between 160° and

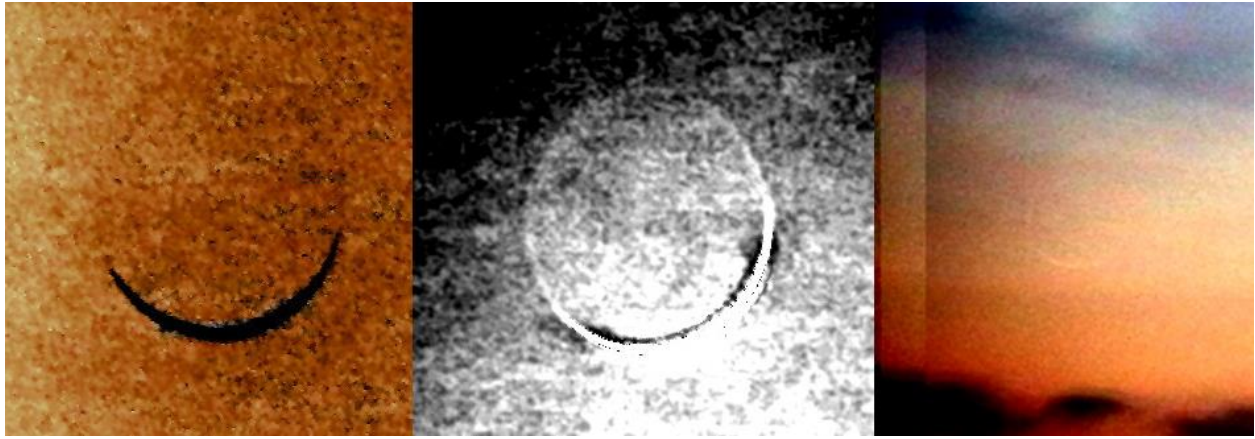


Figure 1: A complete annulus encircles the Earth-lit surface of the Moon in the processed video frames taken at Kula, Turkey in 2006 (left), and Weidenbach, Germany, in 2008 and 2011. Phase angles were 163° , 161° , and 169° (from left to right).

170° . Only few single images show the complete phenomenon without processing (stacking and gamma adjustment). It can be shown that the resulting enhancement of the near-surface brightness is not caused by artifacts, since there is only a correlation with the phase angle and not with the contrast to the Earth-shine. The latter may be the most reliable light source for a comparison.

Quantification of the flux from the dust layer is almost impossible considering atmospheric extinction and scintillation, and unintended scaling by image processing. The signal per pixel of the ring in single images shows a level of several 10% above the ashen light for phase angles of $\sim 162^\circ$, and an enhanced signal of more than 100% for phase angles $\sim 168^\circ$, with errors of the same order as the relative signal. No major distinction to the sunlit crescent in colour has been found, but in cases of minor phase angles the thin ring might be slightly bluer, consistent with an expected higher proportion of small particles at the higher elevation of the sunlit dust. The level seems to be comparable to the forward scattering Jovian ring system [7]. Although phase and colour dependence indicate particle sizes near the range of μm , the latter authors showed the limited uniqueness of statements on such “typical” particle sizes. Virtually all light comes from a single-pixel layer above the surface of the Moon. A dependence of the intensity of the phenomenon on solar high energy radiation has still to be identified.

References

- [1] Zook, H.A., and McCoy, J.E., *Geophys.Res.Lett.* 18, 2117-2120, 1991.
- [2] Wang, X., et al., *Geophys.Res.Lett.* 43, 6103-6110, 2016.
- [3] Rennilson, J.J., and Criswell, D.R., *Moon* 10, 121-142, 1974.
- [4] Stubbs, T.J., et al., *Adv.Sp.Res.* 37, 59-66, 2006.
- [5] Ip, W.-H., *Geophys.Res.Lett.* 13, 1133-1136, 1986.
- [6] Grün, E., et al., *Planet.Sp.Sci.* 59, 1672-1680, 2011,.
- [7] McNally, D., *Quart.J.Roy.Astr.Soc.* 24, 417-429, 1983.
- [8] Burns, J.A., et al., in *Planetary Rings*, ed. R. Greenberg and A. Brahic, Tucson, 200-272, 1984.

Effects of Activation of Sand Grain Surfaces in simulated wind-driven processes on Mars

P. Nørnberg (1), S. J. Knak Jensen (2), H. P. Gunnlaugsson (3), K. Finster (1), E. Bak (1)

(1) Department of Bioscience, Aarhus University, Denmark. (2) Department of Chemistry, Aarhus University, Denmark, (3) CERN, PH Div, CH-1211 Geneve 23, Switzerland.

Abstract

Wind faceted blocks in the Gusev Crater on Mars as well as sand grains on deck of the Spirit rover reveal that sand is moving on the surface of the planet [1]. Simulated wind-driven processes on Mars were performed in the laboratory by tumbling experiments, which imitates the wind erosion of mineral grains. In a series of experiments we have observed that the process produces a huge number of very small particles with a considerable increased surface of mineral/glass compounds [2]. We can show that the activated minerals 1) oxidize iron phases [3], 2) consume gasses such as methane [4], and 3) in a water suspension kill microorganisms [5].

1. Introduction

The tumbling process takes place in a rotation system moving at 30 RPM which is equivalent to saltation with an impact speed of ~ 1 m/sec (fig. 1), in tubes



Figure 1. End over end tumbler.

with a fall length of 20 cm (fig. 2). Laser diffractometry on samples starting with a grain size of 1 mm to 0.125 mm show that there with time is produced a tail of

small particles in a tumbled sample. The color of the sample slightly reddens, and the surface area of the total sample goes from $0.1 \text{ m}^2/\text{g}$ to $23 \text{ m}^2/\text{g}$. When methane is the atmosphere in the of the test tubes we observe that the pressure of the gas is gradually reduced during the tumbling process. When a tumbled sample of quartz or basalt is suspended in water containing bacterial cells, we observe that the cells die over a contact period of 24 hrs.

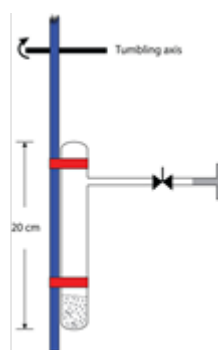


Figure 2. Schematic drawing of tumbling flask.

2. Materials and Methods

The results presented in this paper were produced with commercially available quartz (Merck, 1.07536). The basalt used was Icelandic olivine basalt from Gufunes. The quartz was chosen as an analogue for surface material on Mars because of its simple chemical composition, and because it allowed us carrying out NMR analyses of the reaction products. This would not have been possible if basalt was used instead of quartz due to high iron content, which would corrupt the NMR analyses. Quartz was placed in a borosilicate flask in the tumbling experiments. Magnetite in the experiments is a commercial synthesized laboratory material. Methane is with ^{13}C -methane (Sigma-Aldrich, 490229, 99% enriched) to facilitate NMR investigations.

2. Results and discussion

It is an established fact that the magnetic phase of the Martian soil material is magnetite [6] (Bertelsen et al. 2004). However, as the spectra from the materials suspended in Mars' atmosphere reveal that the red color comes from hematite, the formation process of the hematite is still debated. E.G. it is not clear if water was/is involved in the transformation process.

In our tumbling experiments [3] it is demonstrated that the transformation process of magnetite resulting in hematite (fig. 3) was independent of the atmospheric pressure and composition.

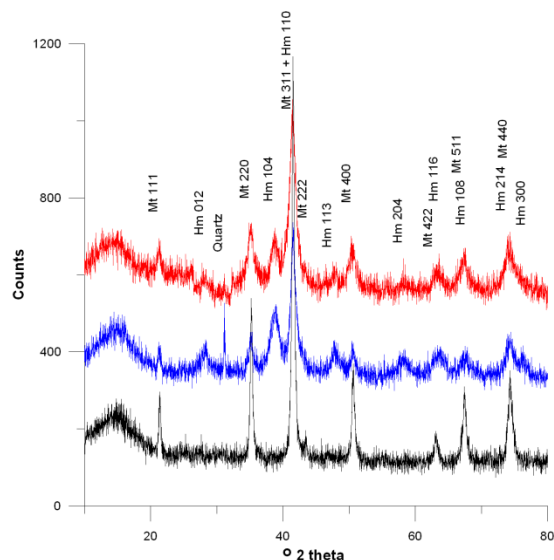


Figure 3. X-ray diffractogram showing transformation of magnetite to hematite.

Methane (CH_4) has been observed in the Martian atmosphere from a satellite orbiting the planet [6], as well as from Earth based telescopes [7]. A significant feature of methane concentrations is that they show a substantial variation in time and space. Detailed snapshot measurements by MSL have shown that the concentration of methane is very low, i.e., 0.18 ± 0.67 ppbv and was considered unlikely related to microbial activity [8]. However, the most recent results from Curiosity at Gale crater (7.2 ± 2.1 ppbv) indicate episodically methane plumes [9]. To reconcile these findings a rapid degradation mechanism is required. Using solid-state ^{13}C and ^{29}Si magic-angle spinning NMR spectroscopies, we have shown that wind driven erosion sequesters methane by forming covalent bonds with methyl groups and propose that this mechanism can be the hitherto undiscovered methane sink on Mars [10].

The reaction of ^{13}C -enriched methane with surface sites of highly active quartz particles is unambiguously demonstrated by the $^{13}\text{C}\{^1\text{H}\}$ CP/MAS and $^{29}\text{Si}\{^1\text{H}\}$ CP/MAS NMR spectra, of which the latter spectra are shown in Fig. 4. In these spectra the cross-polarization (CP) NMR technique transfers ^1H magnetization to either the ^{13}C or ^{29}Si

spins via heteronuclear dipolar couplings and thereby acts as a filter for detecting only ^{13}C and ^{29}Si spin nuclei within a distance less than 3-5 Å to nearby ^1H nuclei. An un-tumbled quartz/methane flask was stored and used as a control for the activation effect.

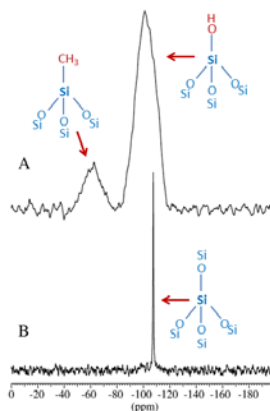


Figure 4: ^{29}Si MAS and CP/MAS NMR spectra

The standard one-pulse ^{29}Si MAS NMR spectrum of the methane-quartz sample in Fig. 4 exhibits a narrow resonance (FWHM = 0.11 ppm) at $\delta(^{29}\text{Si}) = -107.5$ ppm, i.e., the well-known ^{29}Si chemical shift for α -quartz [6] and [7], and thus is assigned to the bulk SiO_2 structure of the sample. More importantly, the ^{29}Si surface sites of the sample are selectively detected in the $^{29}\text{Si}\{^1\text{H}\}$ CP/MAS NMR spectrum (Fig. 2A), which reveals two broadened resonances at -61 and -101 ppm. The high-intensity resonance at -101 ppm originates from ^{29}Si sites associated with hydroxyl groups, following earlier ^{29}Si CP/MAS NMR studies of silica gels. Only this resonance at -101 ppm is observed in a similar spectrum of pure quartz exposed to tumbling in ambient air under the same conditions as used for the $\text{SiO}_2/^{13}\text{CH}_4$ sample (Fig. 2B).

References

- [1] Greeley, R. et al. JGR, 111, 2006
- [2] Nørnberg, P. et al. Aeol.Res. 2014, 77-80.
- [3] Merrison, J.P. et al. Icarus, 2010, 205, 716-718.
- [4] Jensen, S.K. et al. Icarus, 2014, 236, 24-27.
- [5] Bak, E., 2015 ph.d.-thesis, GSST, AU.
- [6] Formisano, V. et al.: Science 2004, 306, 1758-1761.
- [7] Krasnopolsky, V. et al.: Icarus 2004, 172, 537-547.
- [8] Webster, C.R. et al.: Science 2013, 342, 355-356.
- [9] Webster, C.R. et al.: Science 2015, 347, 415-417.
- [10] Jensen, S.K.J. et al.: Icarus 2014, 236, 24-27.

MA_MISS and WISDOM data integration

A. Frigeri (1), M.C. De Sanctis (1), V. Ciarletti (2), F. Altieri (1), D. Plettemeier (3), E. Ammannito (4), S. De Angelis (1) and the MA_MISS team

(1) Istituto di Astrofisica e Planetologia Spaziali - INAF, Rome, ITALY (Alessandro.Frigeri@iaps.inaf.it / Phone: +39-06-4993-4227); (2) LATMOS-IPSL, UVSQ, CNRS/INSU, Guyancourt, France; (3) Technische Universität Dresden, Dresden; (4) Italian Space Agency, Rome, Italy

Abstract

1. Introduction

The 2020 mission of the ExoMars programme will deliver a European rover and a Russian surface platform to the surface of Mars. Among all the experiments onboard the rover, two of them are particularly innovative. In fact, for the first time they will explore the very shallow subsurface of Mars, delivering hyperspectral and electromagnetic imaging of the martian underground at the landing site.

MA_MISS (Mars Multispectral Imager for Subsurface Studies) is the spectrometer which will deliver hyperspectral data from the hole drilled in the Martian ground by the ExoMars Drilling system [1]. The experiment has been funded by the Italian Space Agency (ASI) and developed in Italy by SELEX Galileo.

WISDOM is a ground penetrating radar to study and characterize the structure of the Martian underground [2]. It has been funded by the french Centre National d'Etudes Spatiales (CNES) and german DLR and developed at the Laboratoire Atmosphères, Milieux, Observations Spatiales (LATMOS) in Paris, France.

Herein we introduce the work we are doing in order to delineate the elements for a synergic scientific activity between MA_MISS and WISDOM experiments.

2. MA_MISS and WISDOM Data

The ExoMars rover will land on the selected landing site where all experiments will collect data to characterize the environment and the geologic setting.

MA_MISS is going to deliver hyperspectral data of the borehole produced by the drill while WISDOM is going to collect radar traces which will deliver the dielectric properties of the martian shallow subsurface.

2.1. MA_MISS Hyperspectral Data

MA_MISS [1] is a miniaturized near-infrared imaging spectrometer working in the range 0.4-2.2 μm with 20nm spectral sampling. The spectrometer is placed into the drill shaft and the spectra of a point on the borehole is acquired through a sapphire window.

The acquisition of spectra along the drills' axis and around the borehole results into an hyperspectral image of the wall of the borehole.

This image will define the mineralogic composition of the rocks being investigated and the geometry of geologic structures (dip and dip direction).

2.2. WISDOM Radar Data

The WISDOM Ground Penetrating Radar (Water Ice Subsurface Deposits Observation On Mars, [2]) is one of the experiments onboard ESA-Roscosmos ExoMars Rover mission to Mars. It has been designed to investigate the shallow subsurface of Mars by imaging the subsurface using pulses in the V/U-HF portion of the electro-magnetic spectra.

The depth and the resolution of the survey depends on the operative frequency of the radar and the characteristics of the terrain being penetrated. WISDOM operates at frequencies from 500 MHz to 3 GHz, which results in penetration depths of about 3 meters for dry deposits up to 30 meters in ice and snow. Penetration depths lowers abruptly in case of moist or clay-laden soils and materials with high electrical conductivity.

3. Data integration

Subsurface radar soundings from WISDOM will return subsurface images, or radargrams, generated from two way travel times of echoes depicting the subsurface settings of geologic structures.

While WISDOM data should allow to get an estimate of the permittivity of the subsurface, that is needed to convert measured delays in distances, MA_MISS will provide accurate composition measure-

ments that will be used to calibrate the depths measured by WISDOM.

We are planning to use GIS-based data-models in order to have a location-aware database system where to organize, analyze and visualize data from both instruments.

4. Discussion

MA_MISS data is important to WISDOM as it allow to extract a realistic model of the martian subsurface. At the same time, WISDOM echoes taken along sections (radargrams) or areas (volumes) will extend the punctual measurements of MA_MISS , extrapolating the layering that has been detected and characterized by MA_MISS during a vertical survey.

The practice of data integration is starting by planning hyperspectral imaging of cores taken along WISDOM radar profiles acquired during field tests. This way, the scientific teams of the two instruments will start to refine strategies to integrate data in the most efficient way. This will be critical during mission operations where observation planning will be done on a daily basis.

5. Summary

MA_MISS and WISDOM onboard ExoMars 2020 rover will deliver data from the very shallow subsurface of Mars for the first time ever. The observations from these instruments will be the link of existing dataset acquired from orbital platforms: high resolution mapping imagers and spectrometers and subsurface planetary radar sounders. We are working to optimize the synergy of operation and data integration between the instruments in order to maximize the exploration capabilities and thus the scientific returns of these two experiments.

Acknowledgements

The Italian Space Agency (ASI) has funded the MA_MISS experiment

References

- [1] Coradini, A., et al.: MAMISS: Mars multispectral imager for subsurface studies, *Advances in Space Research*, Volume 28, Issue 8, p. 1203-1208, 10.1016/S0273-1177(01)00283-6, 2001.
- [2] Ciarletti V. et al., PIEEE, 0023-SIP-2010-PIEEE, 2010.

Increased tolerance of *Deinococcus geothermalis* biofilms to space and simulated Martian conditions: The BOSS Experiment of the EXPOSE-R2 Mission

C. Panitz (1,2), J. Frösler (2), J. Wingender (2), H.-C. Flemming (2), E. Rabbow (2), P. Rettberg (2)
Biofilm Centre, University of Duisburg-Essen, Universitätsstraße 5, 45141 Essen, Germany

(1) Uniklinik/RWTH Aachen, Institute of Pharmacology and Toxicology, Wendlingweg 2, 52074 Aachen, Germany

(2) Biofilm Centre, University of Duisburg-Essen, Universitätsstraße 5, 45141 Essen, Germany

(3) DLR (Deutsches Zentrum für Luft- und Raumfahrt e.V.), Institute of Aerospace Medicine, Radiation Biology Department, Research Group Astrobiology, Linder Höhe, 51147 Cologne, Germany

Abstract

In the BOSS experiment (biofilm organisms surfing space), which was performed in the context of the successfully finalized EXPOSE-R2 mission, an international consortium of scientists investigated the ability of a variety of organisms to survive in space and on Mars as a function of their life style. The question in focus is whether there are different strategies for individually living microorganisms (planktonic state) compared to a microbial consortium of the same cells (biofilm state) to cope with the unique mixture of extreme stress factors including desiccation, gamma-, ionizing- and UV radiation in this environment. Biofilms, in which the cells are encased in a self-produced matrix of excreted extra-cellular polymeric substances, are one of the oldest clear signs of life on Earth. Since they can become fossilized they might also be detected as the first life forms on other planets and moons of the solar system and are therefore ideal candidates for astrobiological investigations.

1. Introduction

As an example for the organisms that attended the EXPOSE-R2 mission the results of the flight and mission ground reference analysis of *Deinococcus geothermalis* are presented. *Deinococcus geothermalis* is a non-spore-forming, gram-positive, orange-pigmented representative of the *Deinococcus* family which is unparalleled in its poly-extreme resistances to a variety of environmental stress factors on Earth.

2. Summary and Conclusions

The results demonstrate that *Deinococcus geothermalis* remains viable in the desiccated state over

almost 2 years, whereas culturability was preserved in biofilm cells at a significantly higher level than in planktonic cells. Furthermore, cells of both sample types were able to survive simulated space and Martian conditions and showed high resistance towards extra-terrestrial UV radiation. Additionally results of cultivation-independent investigations of pigment stability, membrane integrity, enzyme activity, ATP content and DNA integrity will be discussed. To conclude biofilms exhibit an enhanced rate of survival compared to their planktonic counterparts when exposed to space and Martian conditions. This seems to indicate an advantage of living as a biofilm when facing the poly-extreme conditions of space or Mars. The findings will contribute to the understanding of the opportunities and limitations of life under the extreme environmental conditions of space or other planets as function of the state of life and aims to contribute to the understanding of the adaptation mechanisms that allow microorganisms to survive in extreme environments, possibly including space and the surface of Mars.

References

- [1] Frösler, J., Panitz, C., Wingender, J., Flemming, H.-C., and Rettberg, P.: Survival of *Deinococcus geothermalis* in Biofilms under Desiccation and Simulated Space and Martian Conditions. *Astrobiology* 17, pp. 431-447, 2017